Applied Physics Letters

Long-wave infrared super-resolution wide-field microscopy using sum-frequency generation

Cite as: Appl. Phys. Lett. **120**, 131102 (2022); https://doi.org/10.1063/5.0081817
Submitted: 10 December 2021 • Accepted: 17 March 2022 • Published Online: 29 March 2022

Richarda Niemann, Sören Wasserroth, Guanyu Lu, et al.

Applied Physics Letters ARTICLE scitation.org/journal/apl

Long-wave infrared super-resolution wide-field microscopy using sum-frequency generation

Cite as: Appl. Phys. Lett. **120**, 131102 (2022); doi: 10.1063/5.0081817
Submitted: 10 December 2021 · Accepted: 17 March 2022 ·
Published Online: 29 March 2022

Richarda Niemann,[1] Sören Wasserroth,[1] Guanyu Lu,[2] Sandy Gewinner,[1] Marco De Pas,[1] Wieland Schöllkopf,[1] Joshua D. Caldwell,[2] Martin Wolf,[1] and Alexander Paarmann[1,a)]

AFFILIATIONS

[1]Fritz-Haber-Institut der Max-Planck-Gesellschaft, Faradayweg 4-6, 14195 Berlin, Germany
[2]Vanderbilt University, Nashville, Tennessee 37235, USA

Note: This paper is part of the APL Special Collection on Optical Nanoprobe Spectroscopy and Imaging.
[a)]**Author to whom correspondence should be addressed:** alexander.paarmann@fhi-berlin.mpg.de

ABSTRACT

Super-resolution microscopy in the visible is an established powerful tool in various disciplines. In the long-wave infrared (LWIR) spectral range, however, no comparable schemes have been demonstrated to date. In this work, we experimentally demonstrate super-resolution microscopy in the LWIR range ($\lambda_{IR} \approx 10$–$12\,\mu$m) using IR-visible sum-frequency generation. We operate our microscope in a wide-field scheme and image localized surface phonon polaritons in 4H-SiC nanostructures as a proof-of-concept. With this technique, we demonstrate an enhanced spatial resolution of $\sim\lambda_{IR}/9$, enabling to resolve the polariton resonances in individual sub-diffractional nanostructures with sub-wavelength spacing. Furthermore, we show that this resolution allows us to differentiate between spatial patterns associated with different polariton modes within individual nanostructures.

In classical light microscopy, the imaging resolution is defined by the diffraction limit of light pointed out by Abbe[1] leading to a spatial resolution limited by the imaging wavelength and the numerical aperture of the objective. Many techniques have been developed and demonstrated to overcome this diffraction limit, such as stimulated emission depletion (STED) microscopy,[2] structured illumination microscopy (SIM),[3] and stochastic optical reconstruction microscopy (STORM).[4] All techniques listed above rely on fluorescence, limiting these approaches to naturally fluorescent or functionalized samples.[5]

In contrast, nanotip-based approaches such as scattering-type scanning nearfield optical microscopy[6] (s-SNOM) and photothermal-induced resonance (PTIR) microscopy[7] have attracted wide attention. These methods provide deeply sub-wavelength imaging that no longer relies on fluorescence, but often suffer from the nanotip influencing the measurement.[8] One alternative to these established approaches is nonlinear-optical frequency mixing, such as sum-frequency generation (SFG),[9] providing label-free far-field access. Here, the light at the resonant imaging wavelength is upconverted with a second, nonresonant light source at a much shorter wavelength providing resonant contrast given by the former, and high spatial resolution defined by the latter.

Specifically, in infrared-visible (IR-VIS) SFG, two laser beams of frequencies ω_{IR} and ω_{VIS} are overlapped spatially and temporally in a second-order nonlinear material, i.e., an interface or a bulk material with broken inversion symmetry, which results in the emission of a third beam of a frequency $\omega_{SFG} = \omega_{IR} + \omega_{VIS}$. A schematic of the process is depicted in Fig. 1(a). SFG is an even-order non-linear technique, which allows the investigation of materials with broken inversion symmetry, therefore making SFG interface specific.[9] Several previous works have employed SFG to perform microscopy, but these approaches were limited to the mid-IR spectral region, where the small ratio of ≤ 4 between IR and VIS wavelengths limits the achievable improvement of the spatial resolution.[10–13]

A large improvement of the spatial resolution can be envisioned when employing SFG microscopy in the long-wave infrared (LWIR) spectral region. In this frequency range, optical phonon resonances in polar crystals leading to the formation of surface phonon polaritons (SPhPs) have recently been investigated extensively.[14,15] In the context of super-resolution microscopy, the confinement of surface polaritons in subdiffractional nanostructures, called localized SPhPs, is of great interest.[16,17] Localized SPhPs are supported between the transversal optical (TO) and the longitudinal optical (LO) phonon frequencies of

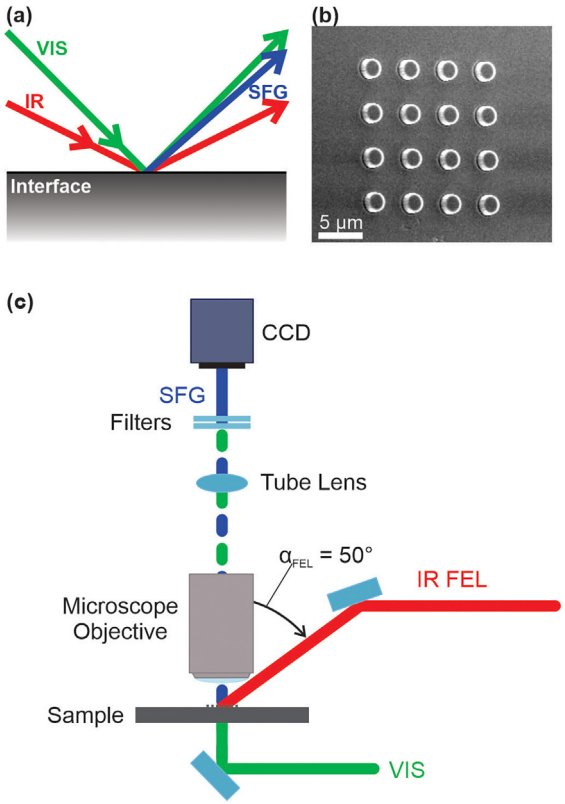

FIG. 1. (a) SFG process. (b) SEM image of a 4 × 4 nanopillar patch, consisting of NPs with a diameter of 2 μm, a period of 5 μm, and a height of 1 μm taken under an angle of 30°. (c) Scheme of the microscope setup. The visible beam illuminates the sample from the back in normal incidence. The IR-FEL beam illuminates the sample from the front under an incident angle of 50°. The SFG light is collected by the microscope consisting of a 50× objective and a 200 mm tube lens. Several filters block the VIS light from entering the CCD camera chip. Here, only the SFG signal is finally imaged.

polar crystals, i.e., within the Reststrahlenband. For these localized SPhPs, the local IR fields are drastically enhanced,[15] which, in consequence, leads to a resonant enhancement of the nonlinear signal emission.[17,18] More specifically, nanopillar arrays made from SiC can support both monopolar and dipolar resonances, characterized by predominantly normal-to-surface and parallel-to-surface optical field enhancements, respectively.[15,16] Previous work demonstrated the concept of LWIR SFG microscopy using a scanning-focus approach,[18] but the spatial resolution was inherently limited by the focus size.

In this work, we achieve super-resolution in LWIR imaging using wide-field SFG microscopy. We employ a tunable narrowband IR free-electron laser (IR-FEL) and a temporally synchronized VIS laser ($\lambda_{VIS} = 527$ nm) for resonant SFG imaging in a home-built wide-field microscope. As a proof-of-concept, we image phonon polariton resonances in 4H–SiC sub-diffractional nanostructures and their collective response.[16–19] Using this approach, we demonstrate a spatial resolution of $\sim\lambda_{IR}/9$. By choosing different IR wavelengths, we can excite monopolar or dipolar SPhP modes in SiC nanopillars.

IR and VIS laser beams illuminate the sample under an incidence angle of 50° and from the backside under normal incidence, respectively. The generated SFG light is collected by an objective and imaged on a camera, see Fig. 1(c). As a mid-IR light source, we use the FEL installed at the Fritz Haber Institute, a high-power laser source offering a tunable wavelength in the mid- to far-IR range (3–50 μm) with a narrow bandwidth on the order of 0.3%. The FEL emission consists of macro-pulses of approximately 8 μs duration generated at a repetition rate of 10 Hz, while each macro pulse contains about 500 micro pulses of few-ps duration at a repetition rate of 55.5 MHz.[20] We excite the sample with the FEL pulses at $\lambda_{IR} \approx 11$ μm with an energy of 5 mJ in the macro pulse and 9 μJ in the micro pulse. The VIS light source is a frequency-doubled 1054 nm table-top 55.5 MHz fiber oscillator (onefive Origami-HP) with a pulse length of 100 fs, providing light at a wavelength of 527 nm with ~10 nJ/pulse on the sample. Both beams are polarized parallel to the incidence plane and focused mildly to spotsizes of ~500 μm (IR) and ~200 μm (VIS), providing a high damage threshold. The temporal overlap of VIS and IR laser pulses is achieved by an RF-based synchronization and verified by optical cross correlation using a phase-matched GaSe crystal. For more details on the timing and synchronization system, see Ref. 21.

The SFG light generated in the sample is collected by the microscope consisting of a 50× long working distance objective (Mitutoyo M Plan Apo 50×, NA = 0.55, working distance wd = 13 mm) and a 200 mm tube lens. The axis of the objective is perpendicular to the sample surface. Behind the objective, the VIS beam at $\lambda_{VIS} = 527$ nm is blocked by several filters (tunable bandpass 547/15, Semrock and single-band bandpass 500/24, Semrock). The SFG light at $\lambda_{SFG} \approx 500$ nm is detected with a high-sensitivity, electron multiplied CCD camera (PI-MAX 4, Teledyne Princeton Instruments). For every image, 100 FEL macro pulses are averaged corresponding to an acquisition time of 10 s/image. The wide field approach provides a field of view of 275 × 275 μm with a 50× magnification.

In order to demonstrate the capabilities of the microscope, we image localized SPhPs in SiC nanopillars (NPs).[16–19] The crystal structure of SiC inherently has a broken inversion symmetry, therefore providing SFG signal from the SiC bulk and the SPhPs modes in the NP volume. In the given geometry, only one unique non-vanishing element $\chi^{(2)}_{xzx} = \chi^{(2)}_{yzy}$ of the second order nonlinear susceptibility $\chi^{(2)}$ tensor can contribute to the nonlinear signal. Thus, our experiment exclusively probes the normal-to-surface components of the local IR fields $E_{IR,z}$.[22] Previous work showed that the enhanced local optical fields at the polariton resonances are responsible for the enhancement of the nonlinear signal[17,18] since the nonlinear susceptibility $\chi^{(2)}$ is featureless in this spectral region.[22] Notably, the resonant frequency of these localized modes depends on the size and shape of the nanostructures as well as on the arrangement and coupling within an array of many individual nanostructures.[15,17,18,23]

For this experiment, all the SiC nanopillar arrays are fabricated into semi-insulating 4H-SiC substrates using a standard electron beam lithography (EBL) process. A 250 nm PMMA 950 A4 layer was spin-coated at 3000 rpm followed by deposition of 10 nm-thick chromium as the conduction layer using thermal evaporation. The patterns were then defined using EBL followed by depositing 100 nm-thick Nickel as a dry etch mask using electron beam evaporation. The SiC nanopillars were etched using reactive ion etching (RIE) using a mixture of O_2 and SF_6 at an etching rate of 375 nm/min, and all the nanopillar structures are etched to 1 μm height. The Nickel mask was removed by aqua regia after the RIE process. Here, we show data based on NP

square arrays ranging from 1×1 to 9×9 pillars. Within each array, the NPs have a period of 5 μm and pillar diameters of 1 μm or 2 μm. An exemplary scanning electron microscope (SEM) image of a 4×4 NP array is shown in Fig. 1(b).

Figure 2(a) shows an SFG image of a 4×4 array of SiC NPs. We resolve the localized SPhP resonance in individual sub-diffractional NPs with sub-wavelength spacing. This provides the opportunity to estimate the spatial resolution of the microscope. For this purpose, we examine the images taken at the IR frequencies according to the monopole resonance of each nanopillar array, i.e., wavelengths between 11.6 and 11.8 μm.[16] Specifically, we analyze horizontal and vertical line profiles, as exemplified by the white lines plotted in Fig. 2(a). The corresponding line profiles are shown in Figs. 2(b) and 2(c). Here, the blue dots show the measured SFG intensity, while the red solid lines show related double-error function fits according to

$$I_{SFG}(x) = \left[\sum_{i=1}^{n} a_i \cdot \left(erf\left(\frac{x+\mu_i+c_i}{\sigma_i * \sqrt{2}}\right) \cdot erf\left(\frac{x+\mu_i-c_i}{\sigma_i * \sqrt{2}}\right)+1\right)\right] + b. \quad (1)$$

Here, a is the intensity amplitude, b is a constant vertical offset, and c is the position of the error function. μ represents the center position of the pillar and σ is the standard deviation of the Gaussian broadening. The spatial resolution R is calculated with $R = 2.9 \cdot \sigma$.[24] For statistical analysis, we imaged nanopillar square arrays of sizes $n \times n$, where $n = 1, \ldots, 9$. Therefore, we have fit parameters of 276 individual nanopillars with a diameter of 1 μm. All fitted values for the horizontal and vertical resolution are plotted in histograms shown in Figs. 2(d) and 2(e). The resulting normal distribution is fitted with a Gaussian (red line) leading to a horizontal resolution of (1.35 ± 0.13) μm and a vertical resolution of (1.39 ± 0.13) μm. The variance of the distribution of extracted resolution values from each NP shown in Figs. 2(d) and 2(e) is likely caused by signal amplitude noise in combination with the finite pixel size of the camera.

With our microscope, we are able to resolve localized SPhP resonances in individual nanopillars with a size and spacing much smaller than the resonant wavelength. These results show clearly that we achieve super resolution of the IR wavelength by a factor of $\sim\lambda_{IR}/9$. The spatial resolution for SFG microscopy is ultimately limited by the diffraction limit of the SFG light, $R_{Abbe} = \lambda_{SFG}/(2NA) = 0.458$ μm with $\lambda_{SFG} = 504$ nm and NA $= 0.55$, which is about 1/3 of the value achieved here. Since the mode volume of the localized SPhPs is finite and on the order of the size of the NPs,[15] the extracted value represents the convolution between the spatial extent of the mode and the resolution of the microscope. Therefore, $R \approx 1.4$ μm is the upper limit of the resolution of the microscope. Additionally, we cannot exclude imperfect alignment of the focusing plane as well as mechanical noise in the home-built microscope as potential contributions to the experimentally achieved resolution.

A spatial resolution on the order of the size of the nanophotonic structures provides the opportunity to study the origin of the SPhP modes. In Figs. 3(a) and 3(b), we present SFG images taken at two different IR wavelengths. The images were taken at the same sample position and show a line of four NPs with a diameter of 2 μm. The white circles indicate the physical pillar size. In Fig. 3(a), we observe a single peak of SFG intensity for each NP, while in Fig. 3(b), we observe a double peak. The different behavior is reflected in the line profiles, Fig. 3(c), corresponding to the white lines in Figs. 3(a) and 3(b), showing a single and a double peak, respectively. This observation is consistent with monopole and dipole modes being excited at these two different wavelengths, shown in Figs. 3(a) and 3(b), as expected from previous work.[15,25] The images are in good agreement with simulations of the electric field distribution of SPhPs in SiC NPs, showing that the monopole mode arises on the top of the nanopillars and the dipole mode arises from the edges of the nanopillars.[15,25]

In our work, we demonstrate IR super-resolution microscopy using sum-frequency generation in a wide-field approach. We image individual sub-wavelength nanostructures with sub-diffractional

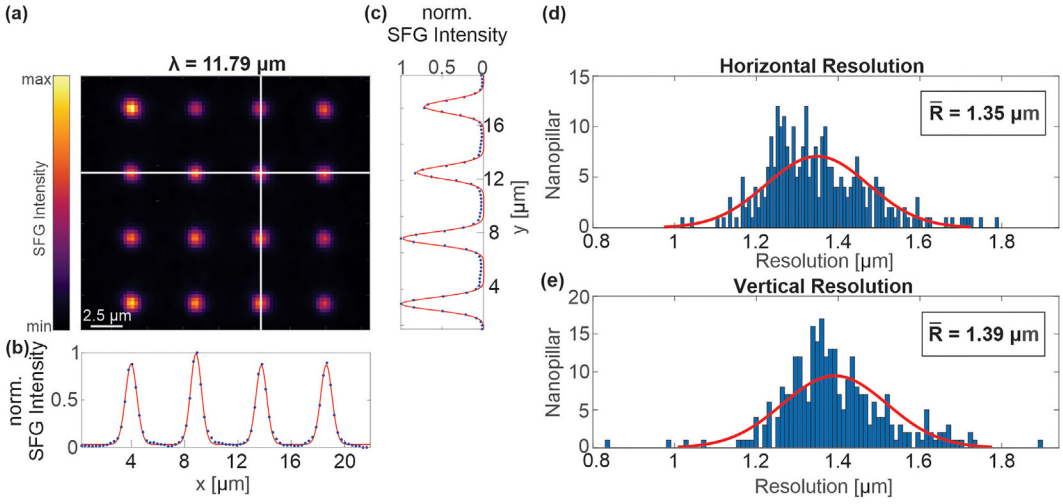

FIG. 2. (a) SFG microscope image of the 4×4 nanopillar array with a pillar diameter of 1 μm. The white lines indicate the position of the line profiles shown in (b) and (c). Blue dots show the measured SFG intensity, and the solid red lines show fits by a series of double error functions, see Eq. (1). (d) and (e) show histograms over all nanopillars (square arrays 1×1 to 9×9) for the vertical and horizontal resolutions. A Gaussian fit gives a resolution of 1.35 and 1.39 μm for horizontal and vertical directions, respectively.

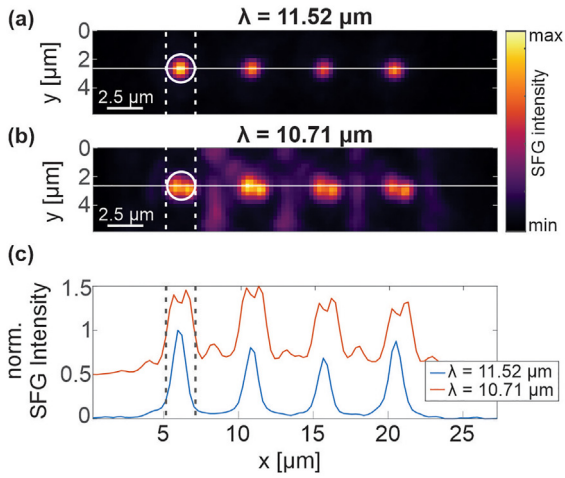

FIG. 3. SFG images of the nanopillars resonant with the (a) monopole and (b) dipole modes at different IR wavelengths. The physical pillar size is indicated by the white circle. (c) Line profiles along the white lines in (a) and (b) are plotted, showing the ability of resolving a two-peak-behavior on top of the nanopillar in the dipole mode in comparison to the monopole mode.

spacing and achieve a resolution of a factor of ∼9 smaller than the wavelength of the probing IR light. With the super-resolution SFG microscope, we are able to distinguish between different SPhP modes, i.e., the monople and dipole mode, in individual SiC NPs. The spatial resolution of $R \approx 1.4\,\mu$m achieved experimentally is three times larger than the theoretical Abbe limit, where likely the finite spatial extent of the localized modes as well as imperfect alignment and mechanical noise contribute to this discrepancy.

In general, the wide-field microscope introduced here opens up a wide range of applications. Beyond nanophotonic problems, our approach further allows us to investigate spatially heterogeneous interfaces in electrochemistry[26] or domain structures in complex oxides,[27] by specifically using vibrational resonance imaging in these systems. In particular, the large tunability of the IR-FEL further into the far-IR will allow us to address many open questions in these areas, while preserving the high spatial resolution. We also note that table-top narrowband LWIR laser sources are being developed,[28] potentially opening up the methodology presented here to a larger user community.

We acknowledge helpful discussion with Martin Thämer, Ben John, and Tuhin Khan (all FHI Berlin). J.D.C. acknowledges support from the U.S. Army Research Office (No. W911NF2110119), while G.L. was supported by a grant from NASA (No. 80NSSC21K0766). Funding for G.L. was provided through an small business technology transfer (STTR) program provided by the National Science Foundation, Division of Industrial Innovation and Partnerships (IIP) (Award No. 2014798). A portion of this research was conducted at the Vanderbilt Institute of Nanoscale Science and Engineering.

AUTHOR DECLARATIONS

Conflict of Interest

The authors have no conflicts to disclose.

DATA AVAILABILITY

The data that support the findings of this study are openly available in Long-wave infrared super-resolution wide-field microscopy by sum-frequency generation—experimental data,, at https://doi.org/10.5281/zenodo.5771605, Ref. 29.

REFERENCES

[1]E. Abbe, "Beiträge zur Theorie des Mikroskops und der mikroskopischen Wahrnehmung," Arch. Mikrosk. Anat. **9**, 413 (1873).
[2]G. Vicidomini, P. Bianchini, and A. Diaspro, "STED super-resolved microscopy," Nat. Methods **15**, 173 (2018).
[3]R. Heintzmann and T. Huser, "Super-resolution structured illumination microscopy," Chem. Rev. **117**, 13890–13908 (2017).
[4]M. Bates, S. Jones, and X. Zhuang, "Stochastic optical reconstruction microscopy (STORM): A method for superresolution fluorescence imaging," Cold Spring Harbor protocols **2013**(2013), (2013).
[5]L. Schermelleh, A. Ferrand, T. Huser, C. Eggeling, M. Sauer, O. Biehlmaier, and G. P. C. Drummen, "Super-resolution microscopy demystified," Nat. Cell Biol. **21**, 72–84 (2019).
[6]H. Heinzelmann and D. Pohl, "Scanning near-field optical microscopy," Appl. Phys. A **59**, 89–101 (1994).
[7]A. Dazzi, "Photothermal induced resonance. Application to infrared spectromicroscopy," Top. Appl. Phys. **118**, 469–503. (2009).
[8]P. Achmari, A. Siddiquee, G. Si, J. Lin, B. Abbey, and K. Shanshan, "Investigating the probe-tip influence on imaging using scanning near-field optical microscopy," OSA Continuum **4**, 1143 (2021).
[9]Y. R. Shen, *Fundamentals of Sum-Frequency Spectroscopy*, Cambridge Molecular Science (Cambridge University Press, 2016).
[10]V. Raghunathan, Y. Han, O. Korth, N.-H. Ge, and E. O. Potma, "Rapid vibrational imaging with sum frequency generation microscopy," Opt. Lett. **36**, 3891–3893 (2011).
[11]A. Hanninen, M. W. Shu, and E. O. Potma, "Hyperspectral imaging with laser-scanning sum-frequency generation microscopy," Biomed. Opt. Express **8**, 4230–4242 (2017).
[12]K. Cimatu and S. Baldelli, "Sum frequency generation microscopy of microcontact-printed mixed self-assembled monolayers," J. Phys. Chem. B **110**, 1807–1813 (2006).
[13]D. M. P. Hoffmann, K. Kuhnke, and K. Kern, "Sum-frequency generation microscope for opaque and reflecting samples," Rev. Sci. Instrum. **73**, 3221–3226 (2002).
[14]J. D. Caldwell, L. Lindsay, V. Giannini, I. Vurgaftman, T. L. Reinecke, S. A. Maier, and O. J. Glembocki, "Low-loss, infrared and terahertz nanophotonics using surface phonon polaritons," Nanophotonics **4**, 44–68 (2015).
[15]Y. Chen, Y. Francescato, J. D. Caldwell, V. Giannini, T. W. W. Maß, O. J. Glembocki, F. J. Bezares, T. Taubner, R. Kasica, M. Hong, and S. A. Maier, "Spectral tuning of localized surface phonon polariton resonators for low-loss mid-IR applications," ACS Photonics **1**, 718–724 (2014).
[16]J. D. Caldwell, O. J. Glembocki, Y. Francescato, N. Sharac, V. Giannini, F. J. Bezares, J. P. Long, J. C. Owrutsky, I. Vurgaftman, J. G. Tischler, V. D. Wheeler, N. D. Bassim, L. M. Shirey, R. Kasica, and S. A. Maier, "Low-loss, extreme subdiffraction photon confinement via silicon carbide localized surface phonon polariton resonators," Nano Lett. **13**, 3690–3697 (2013).
[17]I. Razdolski, Y. Chen, A. J. Giles, S. Gewinner, W. Schöllkopf, M. Hong, M. Wolf, V. Giannini, J. D. Caldwell, S. A. Maier, and A. Paarmann, "Resonant enhancement of second-harmonic generation in the mid-infrared using localized surface phonon polaritons in subdiffractional nanostructures," Nano Lett. **16**, 6954–6959 (2016).
[18]R. Kiessling, Y. Tong, A. J. Giles, S. Gewinner, W. Schöllkopf, J. D. Caldwell, M. Wolf, and A. Paarmann, "Surface phonon polariton resonance imaging using long-wave infrared-visible sum-frequency generation microscopy," ACS Photonics **6**, 3017–3023 (2019).
[19]G. Lu, C. R. Gubbin, J. R. Nolen, T. Folland, M. J. Tadjer, D. Liberato, and J. D. Caldwell, "Engineering the spectral and spatial dispersion of thermal emission via polariton–phonon strong coupling," Nano Lett. **21**, 1831–1838 (2021).

[20]W. Schöllkopf, S. Gewinner, H. Junkes, A. Paarmann, G. von Helden, H. P. Bluem, and A. M. M. Todd, "The new IR and THz FEL facility at the Fritz Haber Institute in Berlin," Proc. SPIE **9512**, 95121L (2015).
[21]R. Kiessling, W. B. Colson, S. Gewinner, W. Schöllkopf, M. Wolf, and A. Paarmann, "Femtosecond single-shot timing and direct observation of subpulse formation in an infrared free-electron laser," Phys. Rev. Accel. Beams **21**, 080702 (2018).
[22]A. Paarmann, I. Razdolski, S. Gewinner, W. Schöllkopf, and M. Wolf, "Effects of crystal anisotropy on optical phonon resonances in midinfrared second harmonic response of SiC," Phys. Rev. B **94**, 134312 (2016).
[23]G. Lu, C. R. Gubbin, J. R. Nolen, T. G. Folland, K. Diaz-Granados, I. I. Kravchenko, J. A. Spencer, M. J. Tadjer, O. J. Glembocki, S. De Liberato, and J. D. Caldwell, "Collective phonon–polaritonic modes in silicon carbide subarrays," ACS Nano **16**, 963–973 (2022).
[24]C. J. Engelbrecht and E. H. Stelzer, "Resolution enhancement in a light-sheet-based microscope (SPIM)," Opt. Lett. **31**, 1477–1479 (2006).
[25]C. R. Gubbin, S. A. Maier, and S. De Liberato, "Theoretical investigation of phonon polaritons in SiC micropillar resonators," Phys. Rev. B **95**, 035313 (2017).
[26]G. Zwaschka, I. Nahalka, A. Marchioro, Y. Tong, S. Roke, and R. K. Campen, "Imaging the heterogeneity of the oxygen evolution reaction on gold electrodes operando: Activity is highly local," ACS Catal. **10**, 6084–6093 (2020).
[27]U. Diebold, S.-C. Li, and M. Schmid, "Oxide surface science," Annu. Rev. Phys. Chem. **61**, 129–148 (2010).
[28]A. Cartella, T. F. Nova, A. Oriana, G. Cerullo, M. Först, C. Manzoni, and A. Cavalleri, "Narrowband carrier-envelope phase stable mid-infrared pulses at wavelengths beyond 10 μm by chirped-pulse difference frequency generation," Opt. Lett. **42**, 663–666 (2017).
[29]See https://doi.org/10.5281/zenodo.5771605 for data repository.